Int. J. Heat Mass Transfer. Vol. 28, No. 4, pp. 807–822, 1985.
Printed in Great Britain

0017–9310/85 $3.00 + 0.00

Natural convection between confocal horizontal elliptical cylinders

WILLARD C. SCHREIBER and SHIVA N. SINGH*
Department of Mechanical Engineering, University of Kentucky, Lexington, KY 40506, U.S.A.

(*Received* 26 *April* 1984 *and in final form* 22 *October* 1984)

Abstract—Steady two-dimensional natural convection in the annulus formed by confocal elliptic cylinders oriented at an arbitrary angle α with respect to the gravity force is formulated in terms of an elliptic coordinate system. The method of spectral series expansion is used to reduce the governing coupled partial differential equations to three sets of second-order ordinary equations. These equations are truncated and then numerically integrated using COLSYS, [1] a finite-element collocation code for boundary value differential equations. Overall equivalent conductivities for the inner surface are determined for the cases with: Rayleigh number based on the gap width, $Ra_L = 100$, 1000, and 10000; eccentricity of the inner ellipse, $e = 0.0$, 0.5 and 1.0; Prandtl number, $Pr = 0.7$; and various angles of orientation, α, of the elliptical annulus with respect to gravity. The special case of $e = 1.0$, corresponding to the convective flow within the annulus formed by an ellipse surrounding a flat plate is investigated in detail. The results are presented in terms of fluid flow patterns, isotherms, graphs of vorticity and local Nusselt numbers on the plate's surface for various values of alpha.

INTRODUCTION

IN THE PAST two decades, buoyancy-driven flows in enclosed spaces have been studied extensively. Many authors have investigated the particular problem of symmetric free convection between concentric, horizontal circular cylinders and concentric spheres. The problem has been approached analytically for small and large Rayleigh numbers by employing various methods to solve the coupled elliptic Navier–Stokes and energy equations.

In order to solve the problem of naturally convective flow in a two-dimensional annulus, Mack and Bishop [2] employed a power series truncated at the third power of the Rayleigh number to represent the stream function and temperature variables. Their results pertain to radius ratios from 1.15 to 4.15, Prandtl numbers between 0.02 and 6×10^6 and Rayleigh numbers less than or equal to 3000. Powe *et al.* [3] have investigated this problem using a finite-difference method for a Prandtl number of 0.7 and a range of radius ratios between 1.16 and 1.7 and cite the experimental work of Liu *et al.* [4], Bishop and Carley [5], Grigull and Hauf [6], and Lis [7] as verification of their results. Kuehn and Goldstein [8] have approached the problem both experimentally and computationally for a circular annulus with a gap width of 0.8 for a range of Rayleigh numbers from 10^2 to 10^5.

The problem of axisymmetric flow between concentric spheres has also been studied extensively. Yin [10] has given experimental results for radius ratios from 1.09 to 2.17 for Grashof numbers from 1.7×10^3 to 1.5×10^7 using both air and water. Singh and Chen [11] have employed a series expansion of the stream function in terms of orthogonal Gegenbauer functions and of the temperature in terms of Legendre polynomials to solve this problem for a radius ratio of 2.0, Prandtl number of 0.02, 0.7, and 6.0, and Grashof number from 10^3 to 2×10^4. Their results match those of Mack and Hardee [12] who have solved the problem using a power series.

Heretofore the problem of eccentrically-shaped annuli has been investigated only briefly. The use of an elliptical coordinate system offers the advantage of its ability to describe a range of annular shapes from a concentric circular cylinder to one whose inner cylinder consists of a finite flat plate. In the latter case no singularities arise at the ends of the plate as they do in a Cartesian coordinate system representation of flow around a finite flat plate. A further advantage of the elliptical coordinate system is its ability to represent an annulus which is asymmetric relative to the force of gravity. The present study in the elliptical annulus oriented at an arbitrary angle with respect to gravity is unique in that asymmetric flows are predicted. Recently Lee and Lee [13] attempted to formulate the free convection problem in terms of elliptical coordinates for the symmetrical cases of oblate and prolate elliptical annuli and have performed experiments for this geometry. That paper treats only the symmetric orientations of the ellipse with respect to the gravity vector and uses the finite difference method to solve the two different equations formulated for the blunt and slender configurations.

BASIC EQUATIONS AND FORMULATION

Consider the steady laminar free convection of an incompressible viscous fluid occupying the region between two horizontal confocal isothermal cylinders at temperatures T_i' and T_o' ($T_i' > T_o'$). The elliptic coordinates (ξ, η) are used such that $\xi = \xi_i$ and ξ_o refer to the inner and outer cylinders respectively. The line common to the minor axes of these elliptic cylinders is inclined at an angle, α, to the gravitational force. The

* To whom correspondence should be addressed.

NOMENCLATURE

All primed quantities are dimensional; all unprimed quantities are dimensionless.

c' half distance between foci of confocal ellipses

e, e' eccentricity of the inner cylinder, $e = c'/r_i$

$f_{sn}, f_{cn}, g_{sn}, g_{cn}, h_{sn}, h_{cn}$ Fourier coefficients, functions of ξ only

$\bar{F}$ body force vector

f_ξ, f_η components of gravitational force vector

g' acceleration of gravity

h' local heat transfer coefficient

$\bar{h}'$ mean heat transfer coefficient

h_1, h_2 scale factors for a general orthogonal coordinate system

k' thermal conductivity

k'_{eq} local equivalent thermal conductivity

$\bar{k}'_{eq}$ mean equivalent thermal conductivity

L gap length, $r'_0 - r'_i$

Nu local Nusselt number, $2h'r'_i/k'$

$\bar{Nu}$ mean Nusselt number, $2\bar{h}'r'_i/k'$

r, r' length of ellipse's major axis, $r = r'/r'_i$

Pr Prandtl number, ν'/α'

R ratio of outer to inner major axes of cylinder, r'_0/r'_i

Ra_i Rayleigh number based on inner cylinder major axis, $g'\beta'(T'_i - T'_0)r'^3_i/\nu'\alpha'$

Ra_L Rayleigh number based on gap width length, $g'\beta'(T'_i - T'_0)(r'_0 - r_1)^3/\nu'\alpha'$

T, T' temperature, $T = (T' - T'_0)/(T'_i - T'_0)$

U_{max}, U'_{max} maximum dimensionless velocity in flow field, $U_{max} = r'_i U'_{max}/\alpha'$

x'_1, x'_2 general orthogonal coordinates of a two-dimensional system.

Greek symbols

α angle with which minor axes of ellipses are oriented with respect to gravity

α' thermal diffusivity

β' volumetric coefficient of thermal expansion

η elliptical angle measured counter clockwise from positive major axis of ellipse

ξ parameter denoting ellipse's size, $r = \cosh \xi$

μ' dynamic viscosity

ρ', ν' density and kinematic viscosity

ψ, ψ' stream function, $\psi = \psi'/\alpha'$

ζ, ζ' vorticity, $\zeta = \zeta'(r'^2_i/\alpha')$.

Subscripts

i value at inner ellipse

o value at outer ellipse.

geometry of the coordinate system is illustrated in Fig. 1.

The governing Navier–Stokes and energy equations in terms of the stream-function, ψ, the vorticity, ζ, and temperature distribution, T, are given as:

$$\frac{\rho'}{h_1 h_2}\frac{\partial(\zeta', \psi')}{\partial(x'_1, x'_2)} = \mu'\nabla^2\zeta' + \nabla x \bar{F}' \tag{1}$$

$$\zeta' = -\nabla^2\psi' \tag{2}$$

$$\frac{1}{h_1 h_2}\frac{\partial(T', \psi')}{\partial(x'_1, x'_2)} = \alpha'\nabla^2 T'. \tag{3}$$

In elliptical coordinates

$$\begin{aligned} x'_1 &= \xi \\ x'_2 &= \eta \end{aligned} \tag{4}$$

$$h_1 = h_2 = \frac{1}{\sqrt{2}}[\cosh 2\xi - \cos 2\eta]^{1/2}. \tag{5}$$

The body force term, $\bar{F}'$, deserves special consideration. Through geometrical arguments (see Fig. 1) the ξ and η components of the body force terms are found to be:

$$f'_\xi = \frac{-\rho' g'[\sin(\alpha)\cos(\eta)\sinh(\xi) + \cos(\alpha)\sin(\eta)\cosh(\xi)]}{[\cos^2(\eta)\sinh^2(\xi) + \sin^2(\eta)\cosh^2(\xi)]^{1/2}}$$

$$f'_\eta = \frac{-\rho' g'[\cos(\alpha)\cos(\eta)\sinh(\xi) - \sin(\alpha)\sin(\eta)\cosh(\xi)]}{[\cos^2(\eta)\sinh^2(\xi) + \sin^2(\eta)\cosh^2(\xi)]^{1/2}}.$$

Employing the Boussinesq approximation in the momentum equation, the nondimensionalized Navier–Stokes and energy equations become:

$$\nabla^2\zeta = \frac{1}{Pr\, h^2}\frac{\partial(\zeta, \psi)}{\partial(\xi, \eta)} - \frac{Ra_L r_i^3}{h^2 L^3} \times \Big[\{\cos(\alpha)\cos(\eta)\sinh(\xi) - \sin(\alpha)\sin(\eta)\cosh(\xi)\}\frac{\partial T}{\partial \xi} - \{\sin(\alpha)\cos(\eta)\sinh(\xi) + \cos(\alpha)\sin(\eta)\cosh(\xi)\}\frac{\partial T}{\partial \eta}\Big] \quad \text{momentum} \tag{6}$$

$$\nabla^2 T = \frac{1}{h^2}\frac{\partial(T, \psi)}{\partial(\xi, \eta)} \quad \text{energy} \tag{7}$$

$$\zeta = -\nabla^2\psi \quad \text{vorticity} \tag{8}$$

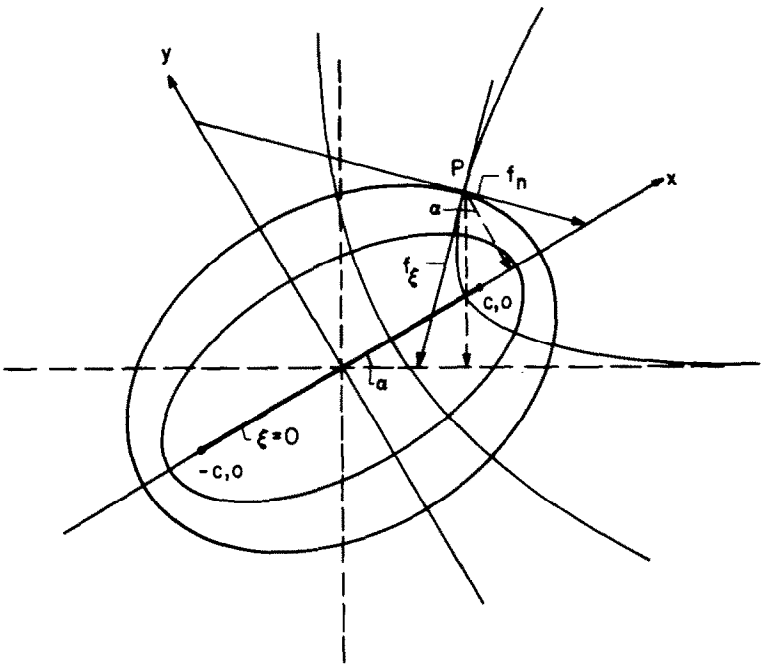

FIG. 1. Elliptical coordinate system with illustration of body force resolved into components, f_ξ and f_η.

where

$$h = h_1 = h_2$$

and

$$\nabla^2 X = \frac{1}{h^2}\left[\frac{\partial^2 X}{\partial \xi^2} + \frac{\partial^2 X}{\partial \eta^2}\right].$$

The boundary conditions are:

$$\psi = \frac{\partial \psi}{\partial \xi} = 0, \quad T = 1, \quad \text{at} \quad \xi = \xi_i \tag{9}$$

$$\psi = \frac{\partial \psi}{\partial \xi} = 0, \quad T = 0, \quad \text{at} \quad \xi = \xi_o. \tag{10}$$

From equations (6)–(10), it is clear that the problem is governed by five parameters: Rayleigh number, Ra_L; Prandtl number, Pr; angle of inclination, α; radius gap width, ($L = \cosh \xi_o - \cosh \xi_i$); and eccentricity parameter, ξ_i. When $\xi_i = 0$, the inner ellipse with an eccentricity of 1.0 represents a flat plate and the problem reduces to that of an annulus enclosed between a flat plate and a confocal ellipse. Thus the use of elliptic coordinates offers the advantage of studying the free convection from the enclosed finite strip as well as for confocal elliptic cylinders.

In order to reduce the partial differential equations (PDEs) to a set of simultaneous ordinary differential equations (ODEs) ψ, ζ, and T are each represented by a general Fourier series

$$\psi = \sum_{n=1}^{\infty} \{g_{sn} \sin(n\eta) + g_{cn} \cos(n\eta)\}$$

$$\zeta = \sum_{n=1}^{\infty} \{h_{sn} \sin(n\eta) + h_{cn} \cos(n\eta)\}$$

$$T = f_o + \sum_{n=1}^{\infty} \{f_{sn} \sin(n\eta) + f_{cn} \cos(n\eta)\}.$$

When these expressions are truncated to $n = N$ terms and then substituted into the governing equations, the use of orthogonality yields $6N + 1$ simultaneous ODEs. The use of the sin/cos Fourier series rather than just the sin or cos series is necessary to represent the asymmetric cases where $0 < \alpha < 90°$. Using a single trigonometric function to represent the dependent variables necessarily imposes the condition of symmetry on the problem. The use of the full Fourier series, however, doubles the number of simultaneous equations which results from its substitution for the dependent variables. For an equal amount of truncation accuracy, therefore, the asymmetric problem's solution requires a good deal more computer storage and CPU time than an equivalent symmetric problem. COLSYS [1], a finite element package designed to solve simultaneous ODEs through the method of collocation, was used to effect the solution.

DISCUSSION OF RESULTS

Since this study examines the natural convection in an annulus whose geometry varies with eccentricity, the

equivalent conductivity, k_{eq}, is the most suitable parameter with which to compare the surface heat transfers of the various elliptically-shaped annuli. The equivalent conductivity is defined as:

$$k'_{eq} = \frac{\left.\frac{\partial T}{\partial \xi}\right|_{convection}}{\left.\frac{dT}{d\xi}\right|_{conduction}}.$$

The Nusselt number is proportional to the overall value of heat transfer rate which consists of both conductive and convective modes; whereas the equivalent conductivity represents the ratio of total heat transfer to conductive heat transfer. Since the geometry of the annulus affects the rate of conductive heat transfer between the inner and outer cylinders, the Nusselt number is not a good indicator of heat transfer when comparing different geometries. For example the overall Nusselt numbers, $\overline{Nu}$, due to purely conductive heat transfer in annuli with the radius gap ratio, $L/2r_i$, of 0.8 in common and whose inner cylinders have eccentricities of 0.0, 0.5, and 1.0 would be 2.094, 2.001 and 1.951 respectively.

The local equivalent conductivity is defined as the ratio of the local Nusselt number on the surface over which a fluid is moving to the local Nusselt number which would be calculated if the fluid were quiescent. The overall equivalent conductivity is given by the ratio of the average Nusselt numbers for either case.

The local Nusselt number is employed to examine the heat transfer characteristics of a flat plate enclosed within an elliptical annulus. This parameter is useful for indicating the heat transfer characteristics of this particular surface is that it indicates the singularities in heat transfer that occur at the finite plate's ends. A derivation of the expression used to calculate the Nusselt number is included as Appendix 1. The local Nusselt number is also used in a comparison with the results from Lee and Lee's work [13].

Several methods are used to verify the resulting solutions. First, a series solution to the first power of the Rayleigh number, Ra, has been obtained as outlined in ref. [2]. A brief description of this solution procedure is presented in Appendix 2. Since the second order expression for a truncation to the second power of Ra_L would contain approx. 5000 terms, the series could be extended only through the first power. The series obtained is felt to be valid to $Ra_L = 100$ at least. Table 1 presents a comparison between the results found using the power series and those determined from the Fourier series solution.

For a second test the results for the coordinate system whose eccentricity is set equal to zero are compared with the solution Kuehn and Goldstein [8] obtained for concentric circular cylinders. The coordinate system presented in the formulation section of this paper has an eccentricity ($e = 1/\cosh \xi_i$) which approaches zero only as ξ_i becomes infinitely large. This formulation employs a *fixed* elliptic coordinate system such that $e = 1.0$ at $\xi_i = 0.0$. If instead, the transformation, $x = r$, $y = \sqrt{(r^2 - e^2)}$, is used to produce a *variable* elliptic coordinate system, the case of concentric cylinders may be obtained by designating the eccentricity, e, as zero. In the variable system of elliptical coordinates, the semi-major axis of the inner ellipse is equal to one regardless of the inner ellipse's eccentricity. The variable elliptic coordinate system might be used for the entire range of eccentricities except that it exhibits singularities when the inner cylinder has an eccentricity of 1.0 and so it cannot represent the case of an inner ellipse as a flat plate.

Table 2 compares the local equivalent conductivities obtained using the variable elliptic system with zero eccentricity to the results for the concentric circular cylinders. The difference between the solutions using both the variable and the fixed coordinate systems both with their eccentricities set to 0.5, was found to be negligible and is not presented in this report.

Another comparison is that made with the results of the works of Lee and Lee [13] and of Lin and Chao [14]. For this comparison the local Nusselt number is determined for the oblate elliptical cylinder whose minor axis is one-half the length of the major axis. As noted by Lee and Lee, when the outer cylinder is extended far from the inner, the flow around the inner closely approximates that around an elliptic cylinder in an infinite medium. Therefore, in the present case, the

Table 1. Comparison between power series solution and Fourier series solution truncated at the fourth term for: $\alpha = 45°$; $e = 1.0$; $Ra_L = 100.0$

	Elliptical angle (η)							
	0	$\frac{\pi}{4}$	$\frac{\pi}{2}$	$\frac{3\pi}{4}$	π	$\frac{5\pi}{4}$	$\frac{3\pi}{2}$	$\frac{7\pi}{4}$
$r = 1.0$								
Fourier	0.851	0.841	0.920	1.034	1.068	1.075	1.015	0.902
Power	0.832	0.817	0.886	1.011	1.059	1.075	1.005	0.880
$r = 2.6$								
Fourier:	1.108	1.135	1.042	0.877	0.818	0.807	0.884	1.035
Power:	1.098	1.122	1.035	0.869	0.793	0.769	0.857	1.022

Numbers are local equivalent conductivities.

Table 2. Comparison of results obtained using the method outlined in the present paper for concentric circular cylinders with those results obtained by Kuehn and Goldstein [8].

	θ^* (degrees)							
	0	30	60	90	120	150	180	$\overline{k_{eq}}$
Inner cylinder								
Present paper	0.43	0.89	1.66	2.32	2.64	2.70	2.80	1.974
Ref. [8]	0.37	0.90	1.64	2.33	2.70	2.85	2.90	2.010
Outer cylinder								
Present paper	4.86	4.09	2.71	1.56	0.70	0.25	0.16	1.974
Ref. [8]	5.35	4.10	2.72	1.54	0.68	0.26	0.14	2.005

* θ equals zero at top of cylinder. $Ra_L = 10000$; $Pr = 0.7$; $L/2r_i = 0.8$.

ratio of the major axis of the outer ellipse to that of the inner ellipse is 20.0. Ra_D, the Rayleigh number whose characteristic length is the inner cylinder's major axis, is set at 100.0 to correspond with Lee and Lee's work. The Prandtl number used is 0.72.

The results of this comparison are shown in Fig. 2. Also included in this figure are the results of the case where Ra_D is assigned the value of 24.0 instead of 100.0. As noted by Lee and Lee a low Rayleigh number yields a higher value of $Nu/Ra_D^{1/4}$ than that predicted by the boundary-layer solution. This trend is illustrated by the results found using $Ra_D = 24.0$. It is noted that the value for $Nu/Ra^{1/4}$ found in the present work are consistently higher than those reported by Lee and Lee.

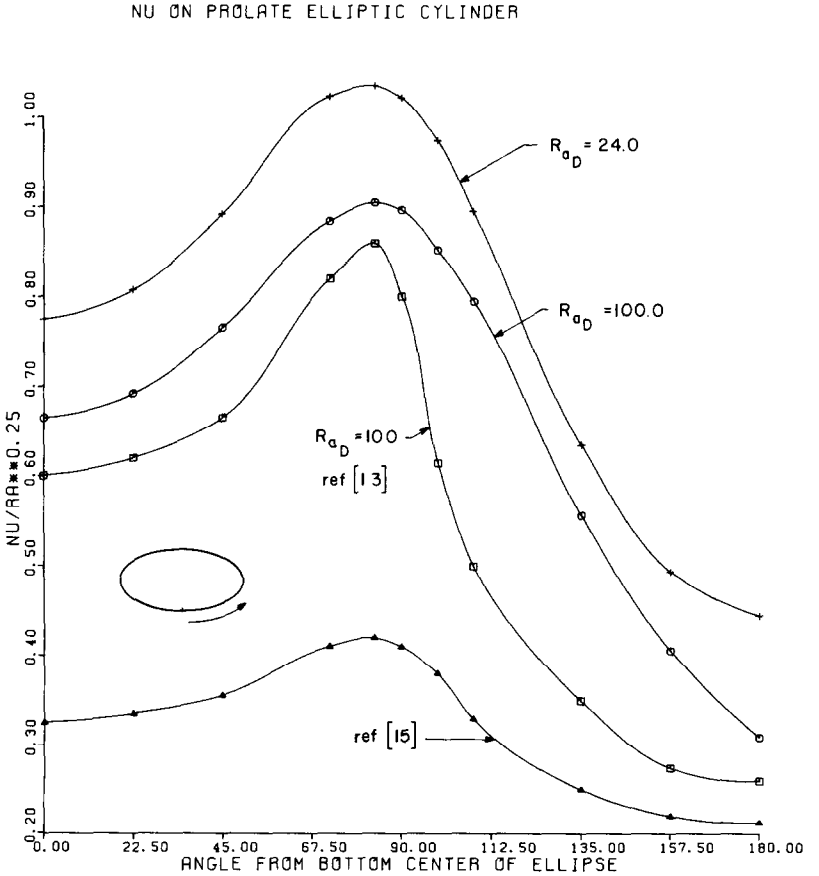

FIG. 2. $Nu/Ra^{1/4}$ predicted by Lee and Lee [13], Lin and Chao [14], and present work for buoyantly-driven flow around an oblate cylinder whose major axis is twice the length of the minor. $Pr = 0.72$; Ra_D, Rayleigh number is based on a characteristic length of the major axis.

A possible explanation for this discrepancy might be found in the definition of the Rayleigh number. If Lee and Lee had defined the characteristic length in the determination of the Rayleigh number as the semi-major axis instead of the major axis then Ra_D would be 800.0 instead of 100.0 and one would expect consistently lower values of $Nu/Ra^{1/4}$ than if Ra_D were 100.0

The fluid flow patterns and isotherms for some of the cases examined in this study are illustrated in Figs. 3–10.

The parameters common to these illustrations are: $Ra_L = 10{,}000$, $Pr = 0.7$, $e = 1.0$ and gap length ratio, $L/2r_i = 0.8$. Since, in general, these flows cannot be represented by a boundary-layer approximation, plots of velocity profiles vs angular coordinates are inappropriate for representation of flow characteristics. Instead plots of the local Nusselt number and of the vorticity on the flat plate's surface better characterize the nature of these flows (Figs. 11–14). The overall equivalent conductivities for all the cases examined are listed in Table 3.

The hydrodynamic and thermal characteristics of the case where $\alpha = 0°$ (Figs. 3 and 4) are entirely symmetric. For $\alpha = 2°$ (Figs. 5 and 6), the resulting flow field demonstrates that the symmetric flow pictured in Fig. 3 is unstable to small changes in the plate's orientation with respect to gravity.

The marked difference between the symmetric flow for $\alpha = 0°$ and the asymmetric flow for $\alpha = 2°$ can be analyzed using the plots of wall vorticity and local Nu at the inner surface. Figures 11 and 13 portray the

Table 3. $\overline{k_{eq}}$ for all cases examined in this paper

		Ra		
e	α (degrees)	100	1000	10,000
0.0	—	1.001	1.082	1.974
0.5	0	1.114	2.136	3.609
0.5	45	1.124	2.154	3.660
0.5	90	1.134	2.183	3.724
1.0	0	1.001	1.295	2.301
1.0	2	1.005	1.349	2.398
1.0	5	1.006	1.356	2.449
1.0	10	1.007	1.378	2.540
1.0	45	1.019	1.605	2.979
1.0	85	1.030	1.706	3.142
1.0	90	1.038	1.718	3.164

$L/2r_i = 0.8$; $Pr = 0.7$.

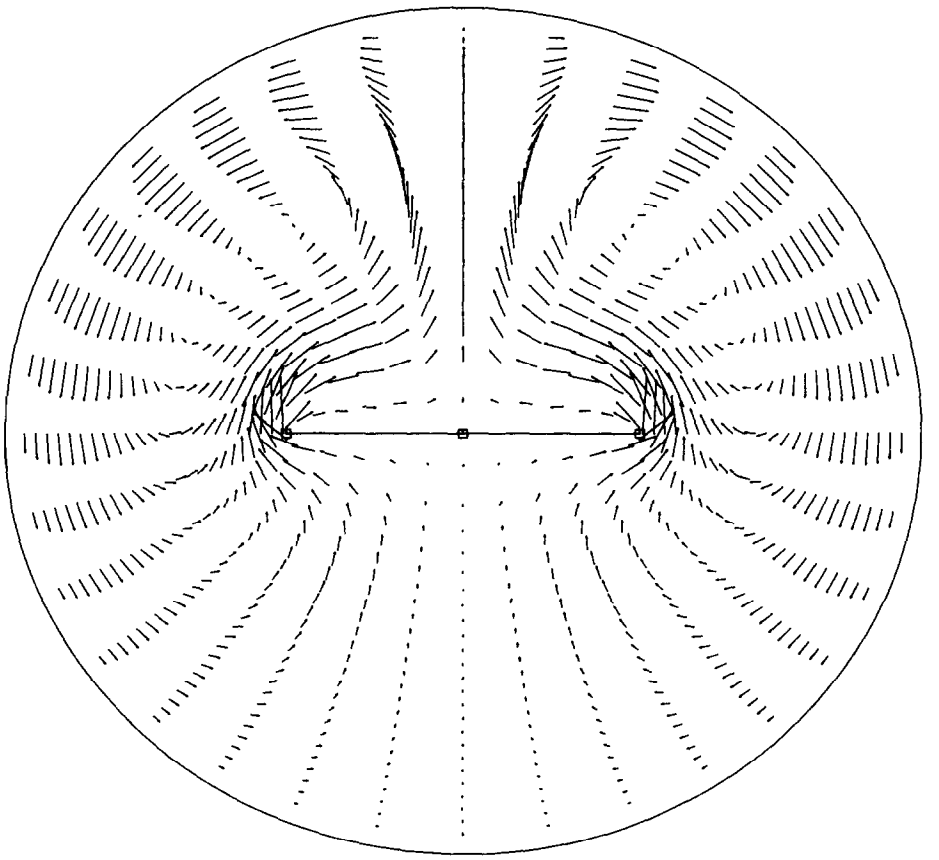

FIG. 3. Velocity field: $Ra_L = 10{,}000$; $Pr = 0.7$; $e = 1.0$; $L/2r_0 = 0.8$; $\alpha = 0°$.

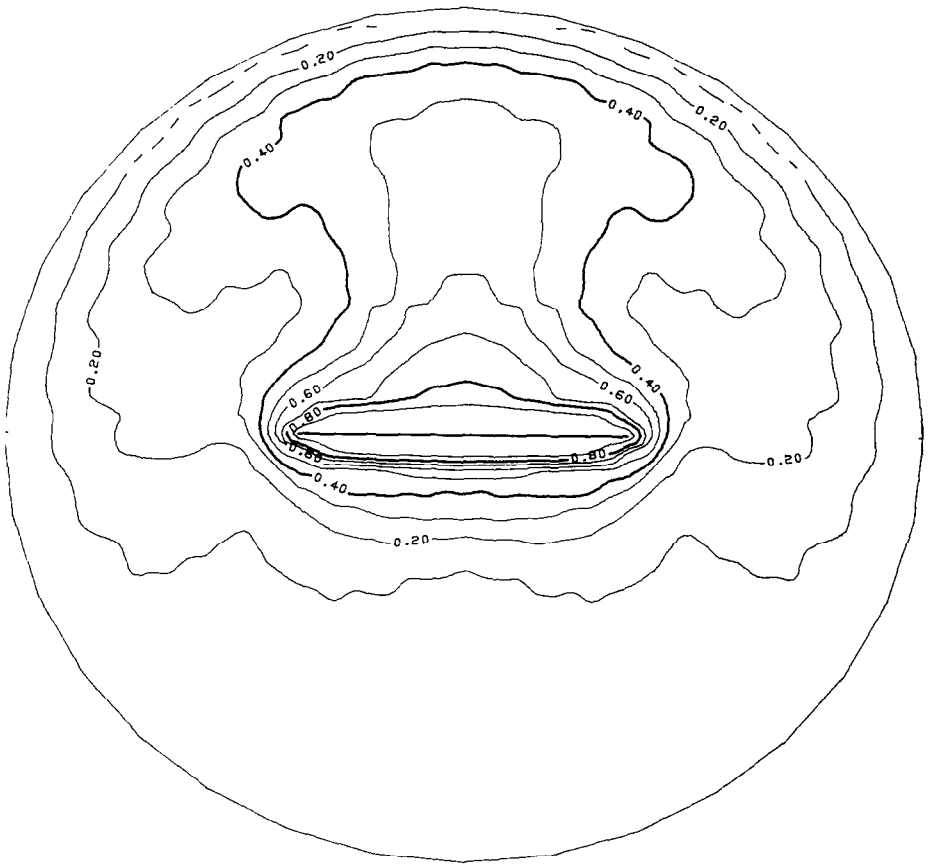

FIG. 4. Isotherms corresponding to case shown in Fig. 3.

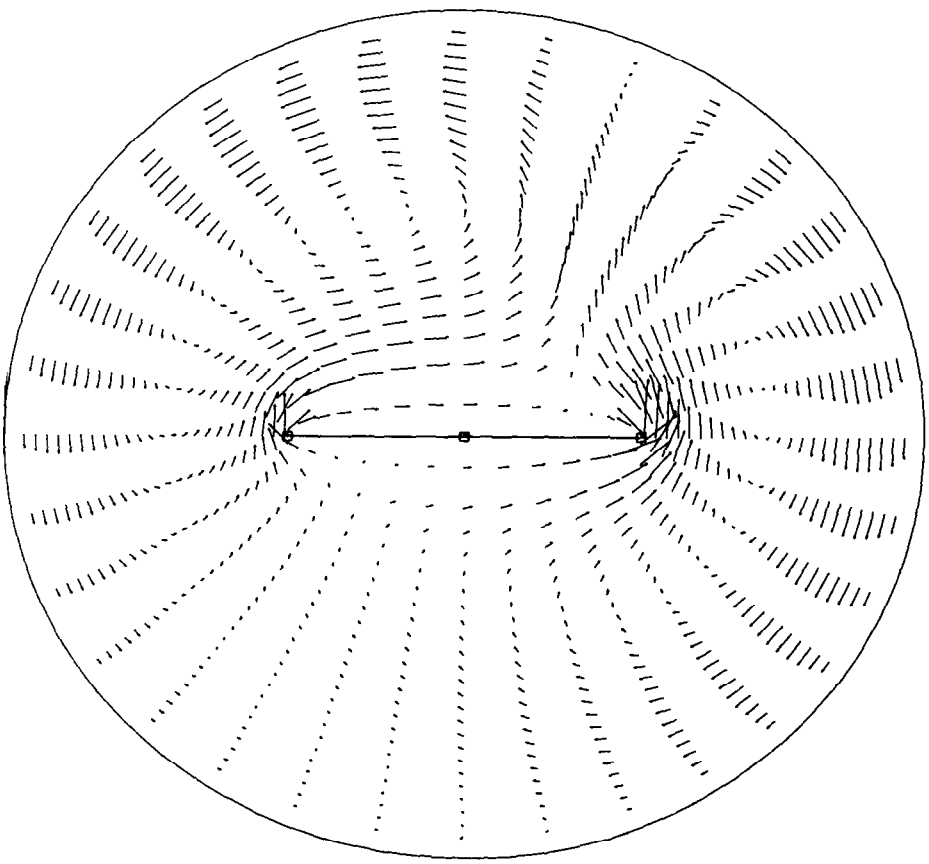

FIG. 5. Velocity field: parameters same as in Fig. 3 except $\alpha = 2°$.

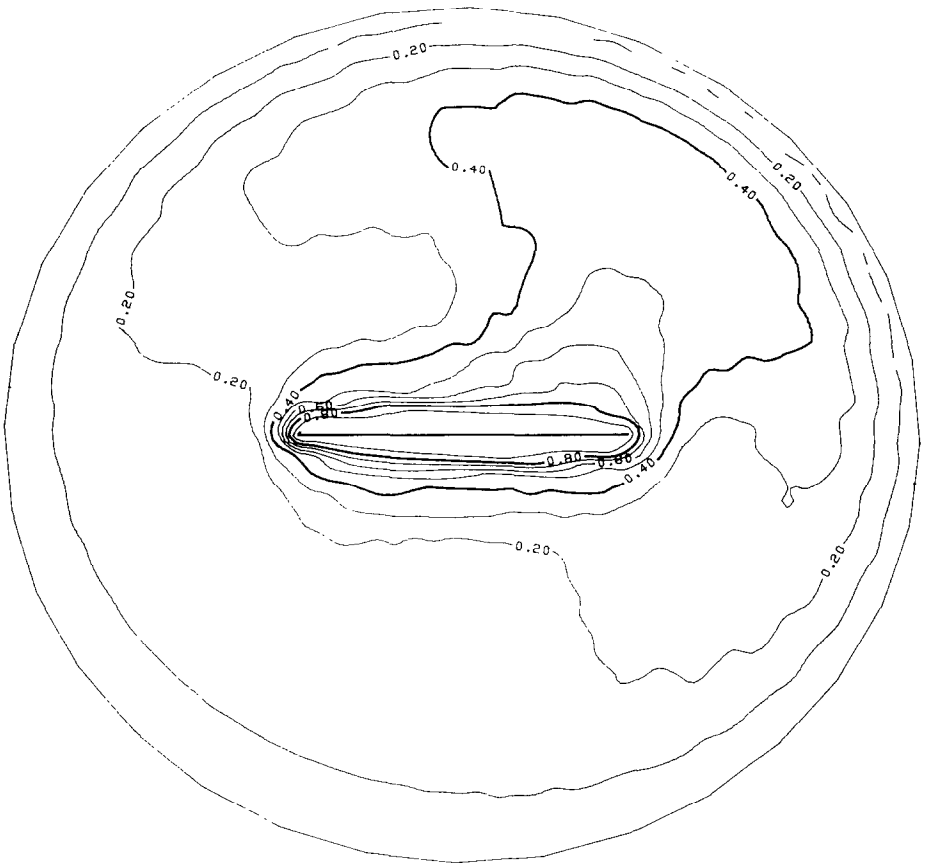

FIG. 6. Isotherms corresponding to case shown in Fig. 5.

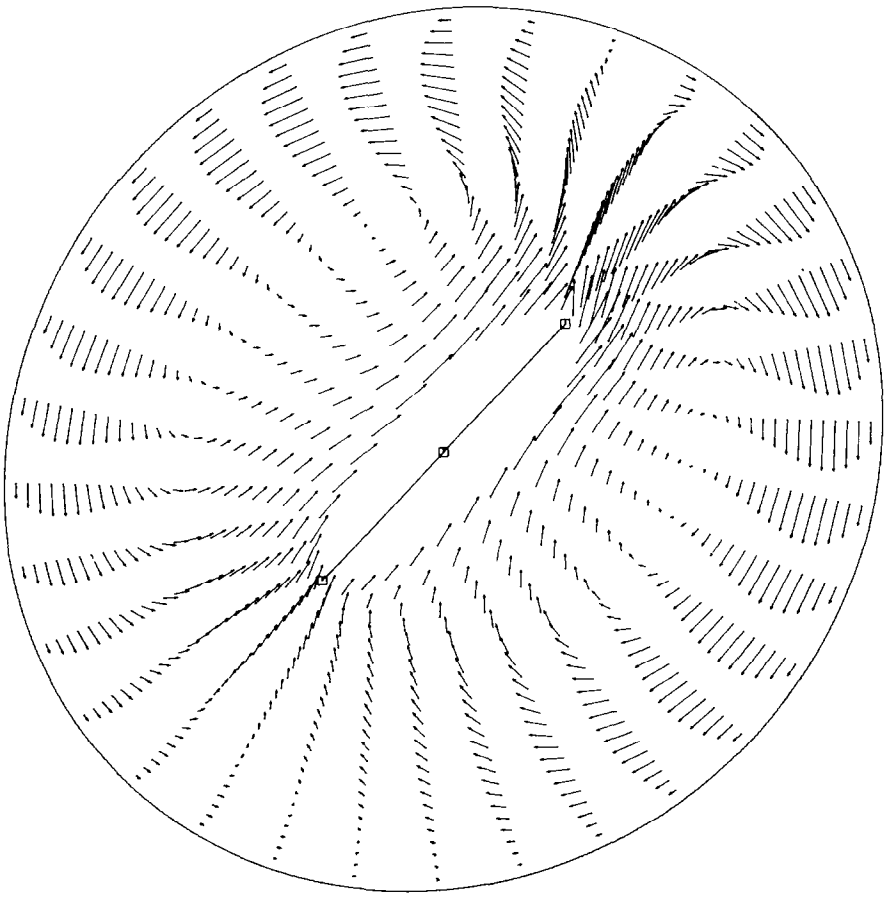

FIG. 7. Velocity field : parameters same as in Fig. 3 except $\alpha = 45°$.

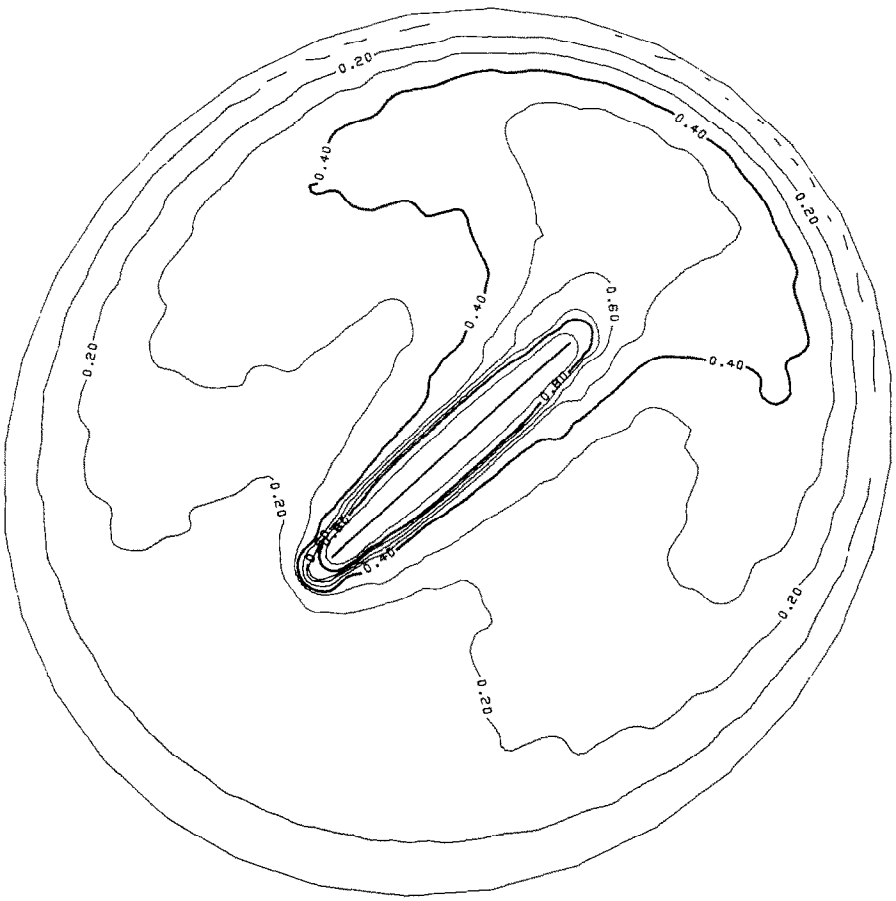

FIG. 8. Isotherms corresponding to case shown in Fig. 7.

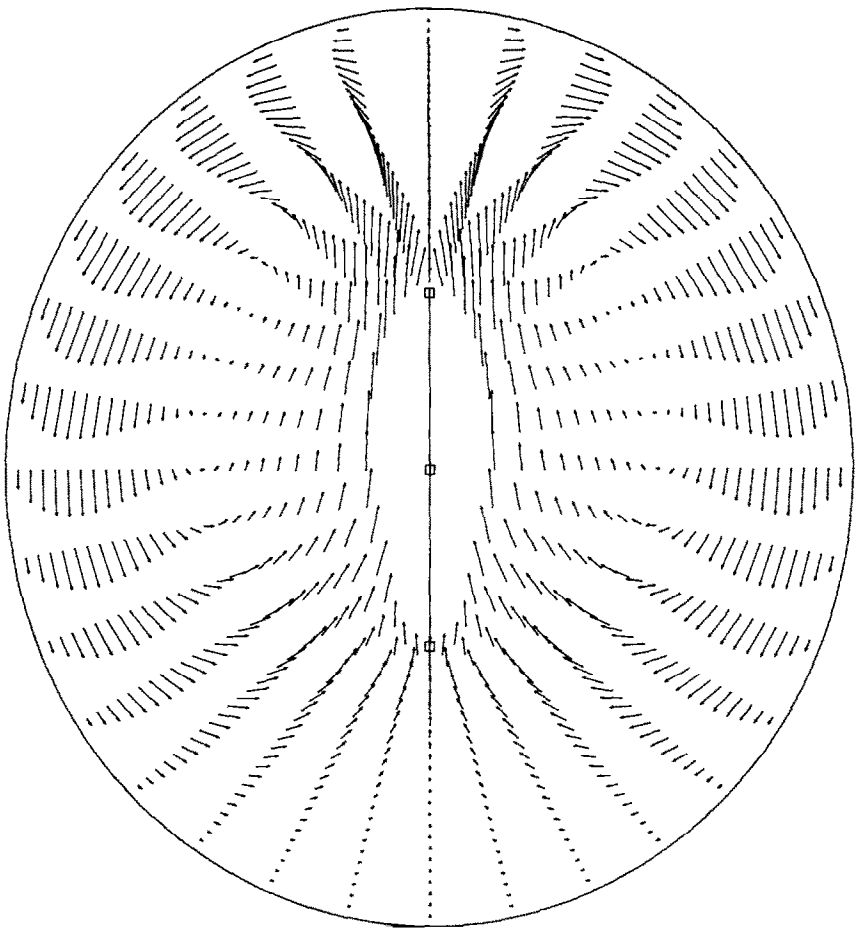

FIG. 9. Velocity field: parameters same as in Fig. 3 except $\alpha = 90°$.

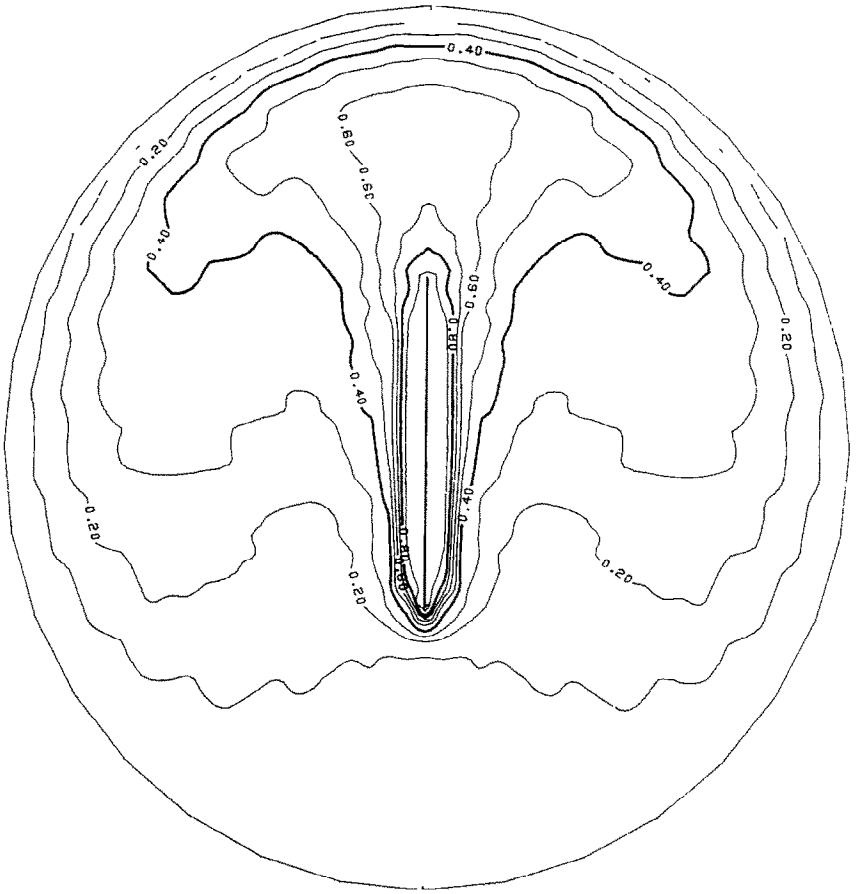

FIG. 10. Isotherms corresponding to case shown in Fig. 9.

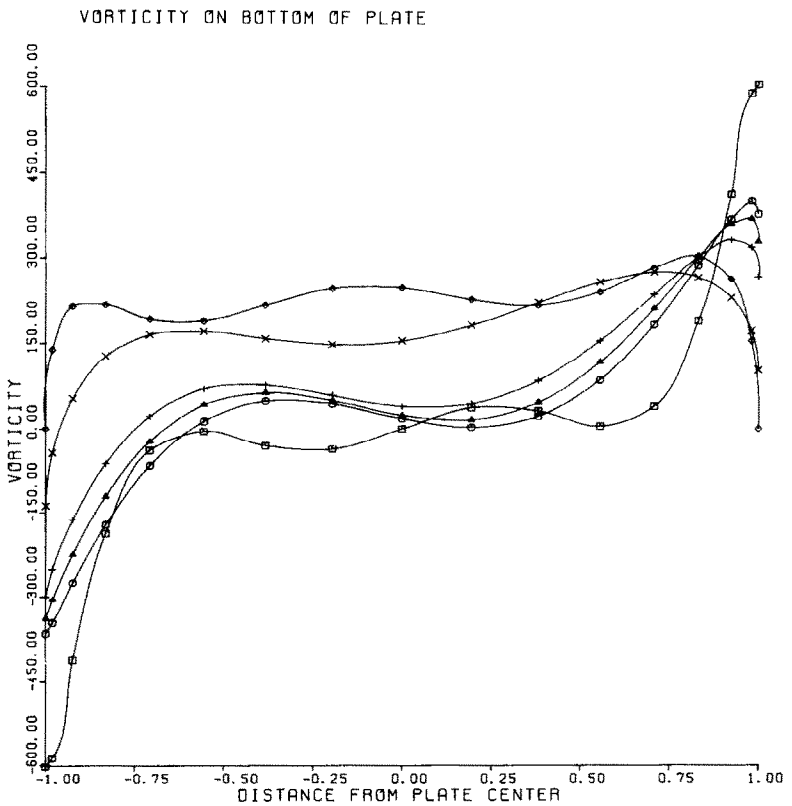

FIG. 11. Vorticity on the plate's lower surface: $Ra_L = 10{,}000$; $Pr = 0.7$; $e = 1.0$; $L/2r_0 = 0.8$; $\alpha = 0, 2, 5, 10, 45, 90°$.

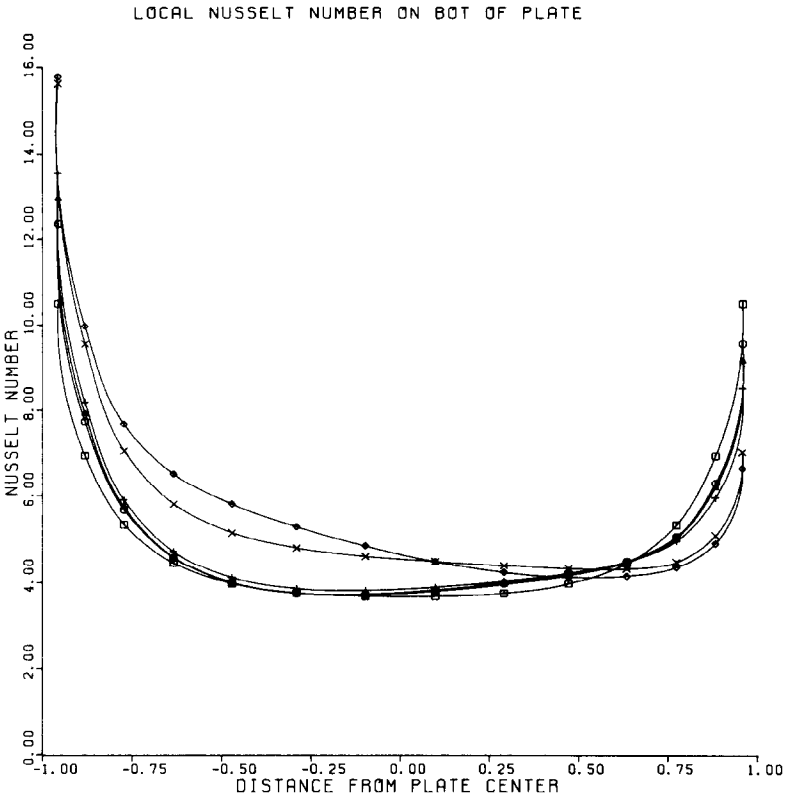

FIG. 12. Local Nusselt number on the plate's lower surface; parameters same as in Fig. 11.

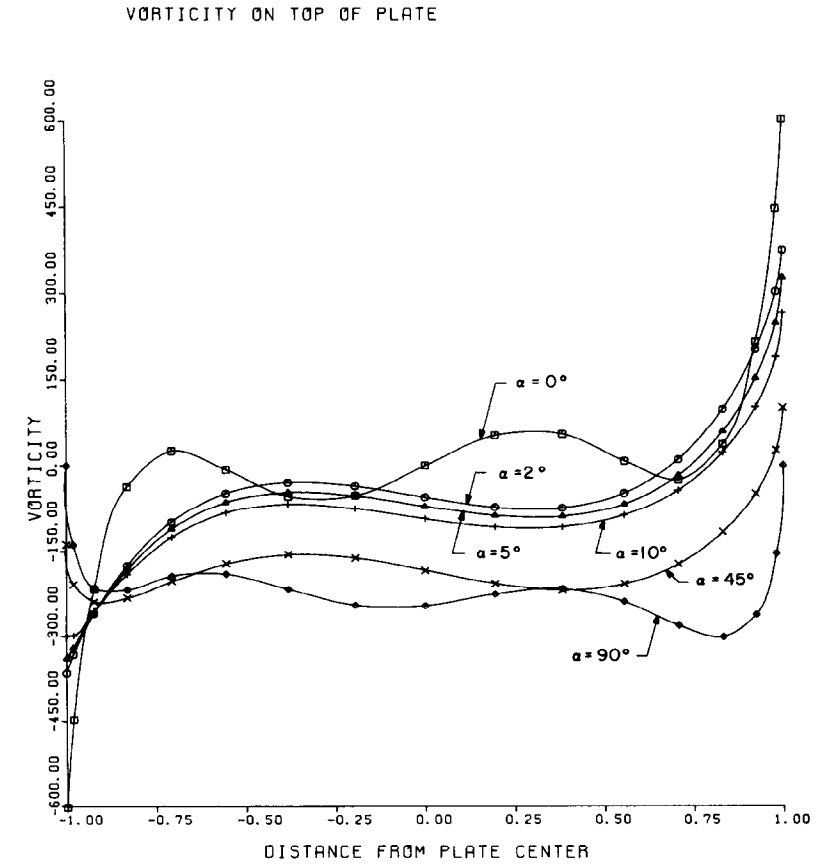

FIG. 13. Vorticity on the plate's upper surface; parameters same as in Fig. 11.

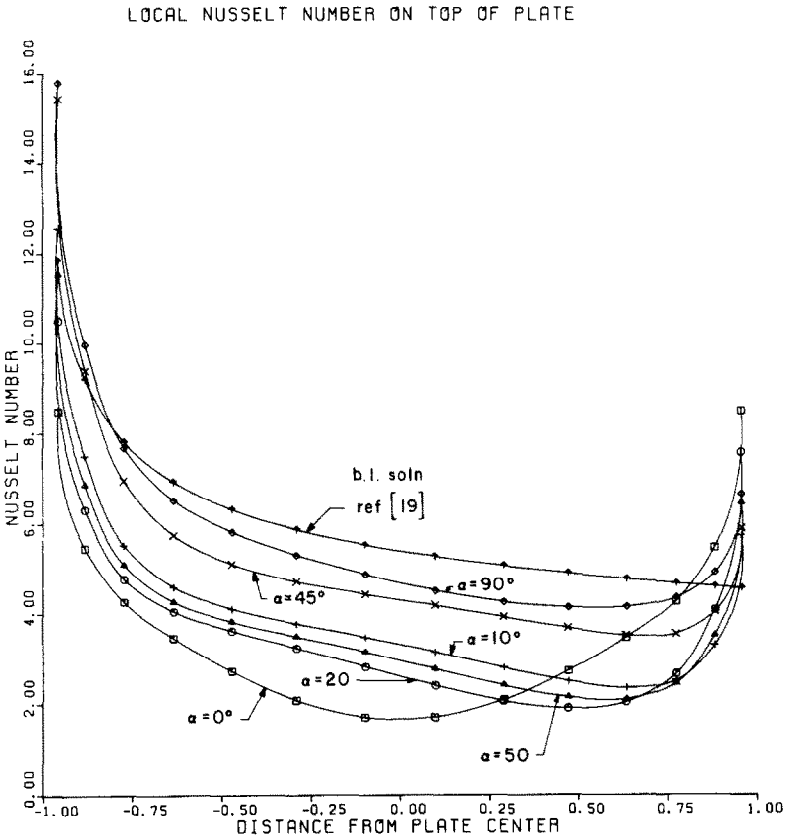

FIG. 14. Local Nusselt number on the plate's upper surface; parameters same as in Fig. 11.

difference between the flows for $\alpha = 0°$ and $\alpha = 2°$. The magnitude of the vorticity, ζ, for the horizontal plate reaches a maximum of almost 600 at the plate's ends; whereas when the plate is tilted 2°, the magnitude of the vorticity at the plate's ends is about 400. On the top surface of the plate, the flow patterns of the two cases exhibit marked differences. The plot of vorticity for the horizontal plate indicates two small recirculation zones on the plate's upper surface. These recirculation zones are weak and are confined to an area very near the plate's surface. They are not portrayed in the velocity pattern shown in Fig. 3. For $\alpha = 2°$, however, these recirculation zones disappear and the flow separates about 1/8 of the plate's length from the upper most edge.

On the plate's lower side, for the case of $\alpha = 0$, the magnitude of the vorticity reaches minima between the centered stagnation point and the plate's ends. These minima result from the interaction of the flow of fluid being entrained from below the plate beyond the plate's ends with the outgoing flow. At these points the flow stagnates and almost separates; the rapid flow about the plate's ends creates a low pressure which causes the outgoing flow to quickly recover. In the case of $\alpha = 2°$ the flow stagnates about 1/4 of the plate's length from the lower end. The shear stress rapidly increases as the flow moves along the plate's bottom toward the lower end. As the flow moves toward the plate's upper end, however, it almost stalls slightly beyond the plate's center due to the incoming fluid which is being entrained.

That the flow configuration about the horizontally oriented plate is unstable to slight angular perturbations can be seen by studying the effect of a small angular tilt from that position. This effect is demonstrated with a comparison of the surface vorticity of the case for $\alpha = 0$ and 2° (Figs. 11 and 13) and of the flow fields for each case (Figs. 3 and 5). When the plate is tilted to a larger angle ($\alpha = 5, 10°$) the change in the flow field as evidenced by the surface vorticity is small. Even an angle of 45° produces the same trend in surface vorticity development except at the leading edge on the plate's top, where the vorticity experiences a decrease instead of the sharp increase seen for the more horizontal plate's orientation.

The flow field about the plate oriented at 45° exhibits, to a large degree, the same characteristics of the vertical plate. On the vertical plate's upper end the flow up the plate experiences a momentary increase in vorticity before the vorticity's sudden decrease to zero at the plate's tip. This increased vorticity at the plate's upper end can be attributed to the transition of the boundary layer from that along the plate's surface to the buoyant jet which forms eventually in the plate's wake.

Plots of the local Nusselt number along the plate's

surface (Figs. 12 and 14) demonstrate the effect of the fluid's flow characteristics on the heat transfer at the plate's surface. On the top surface the minimum value of Nu corresponds to the location of the flow's point of separation. Toward the plate's ends the heat transfer approaches infinity since the conductive heat transfer for a surface with a zero radius of curvature must be infinite.

Due to the proximity of the outer boundary to the surface of the flat plate, the flow around the flat plate is not expected to be equivalent to that of an external flow. It is interesting to compare the plot of the local Nusselt number as predicted by boundary-layer theory for a vertical semi-infinite plate to that found in the present study. For the vertical plate, Ede [15] gives the correlation:

$$Nu_x = \frac{3}{4}\left[\frac{2Pr}{5(1+2Pr^{1/2}+2Pr)}\right]^{1/4}[Gr_x\, Pr]^{1/4}.$$

Substituting the parameters in the present case, this formula is used to determine a curve in Fig. 14. It is noted that except very close to the plate's upper edge the prediction is close to the curve for $\alpha = 90°$.

In Table 3, the overall equivalent conductivities for all cases examined in this study are presented. As noted previously the results for the geometry of concentric cylinders (eccentricity of inner and outer ellipses equals zero) matches the results obtained by Kuehn and Goldstein fairly closely. At the other geometrical extreme, the case where the inner ellipse is a flat plate, it is observed that $\overline{k_{eq}}$ continually increases as the system is rotated from a system whose minor axis is horizontal to gravity to that which is vertical. The maximum rate of increase occurs as the plate is tilted from the horizontal position. The increase in $\overline{k_{eq}}$ from $\alpha = 85$ to 90° is only 15% of the increase if the plate is tilted from $\alpha = 0$ to 5°. The flow patterns are observed to change markedly when the elliptical annulus is tilted slightly from the horizontal orientation and to change little as the plate is rotated from $\alpha = 45$ to 90°. This evolution of the buoyantly-driven flow with increase in α serves as an explanation of the progression of increase in $\overline{k_{eq}}$.

In the annulus whose inner ellipse has an eccentricity of 0.5, the ratio of $\overline{k_{eq}}$ of the vertical to the horizontal orientation is seen to be less than that of the system whose inner surface is a flat plate. As might be expected

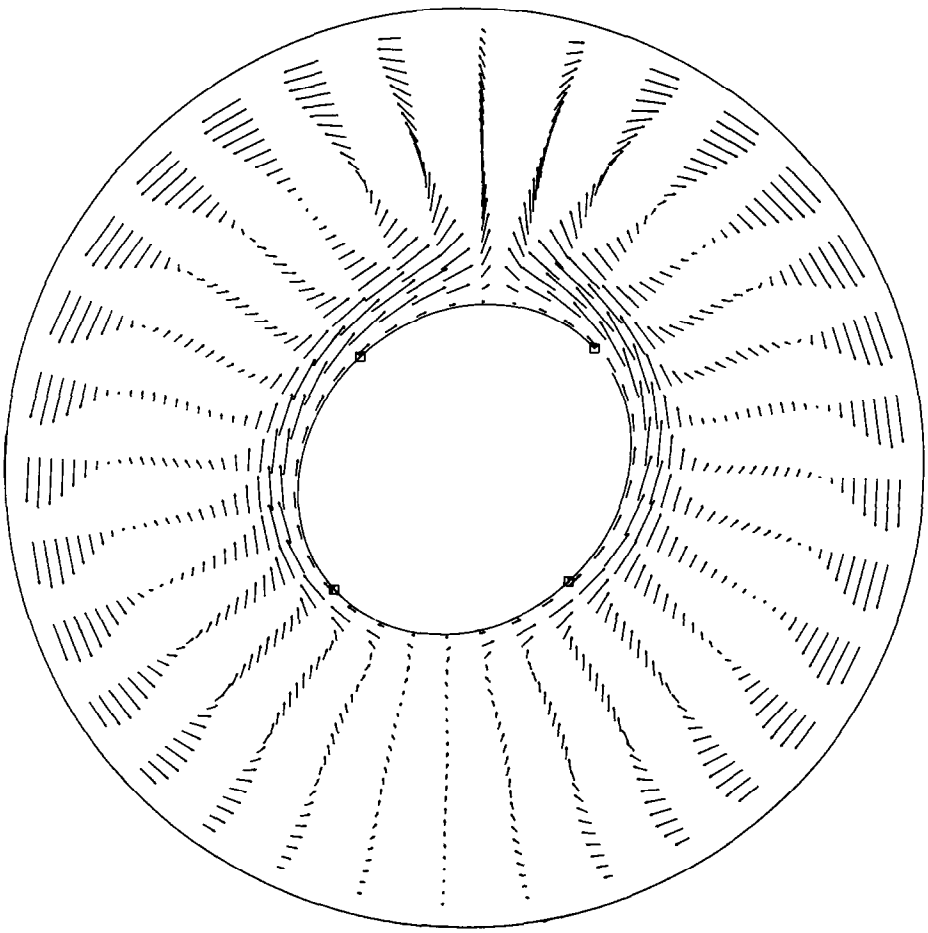

FIG. 15. Velocity field: $Ra = 10{,}000$; $\alpha = 45°$, $e = 0.5$, $L/2r_0 = 0.8$; $Pr = 0.7$.

the less the eccentricity of the annulus the smaller the change in $\overline{k_{eq}}$ with the variation of angular orientation.

The most striking feature observed in Table 3 is the relatively large value of $\overline{k_{eq}}$ for the annulus whose inner ellipse has an eccentricity of 0.5. Figure 15 features the flow field which arises from this particular case. The slightly eccentric geometry seems to enhance the convective heat transfer between the surfaces enclosing the annulus. The corresponding flow field in the concentric circular annulus ($e = 0.0$) is illustrated in Fig. 10 of ref. [9]. A comparison of the two figures reveals that eccentricity in the annulus causes the existence of four convection cells rather than the two found in the circular annulus. This added circulation causes an increase in heat transfer for the slightly eccentric annulus.

REFERENCES

1. O. Ascher, J. Christiansen and R. D. Russell, A collocation solver for mixed order systems of boundary value problems, Tech. Rep. 77-13 Dept. Computer Sci., Univ. B.C., Vancouver, Canada.
2. L. R. Mack and E. H. Bishop, Natural convection between horizontal concentric cylinders for low Rayleigh numbers, *Q. Jl Mech. appl. Math.* **21,** 223–241 (1968).
3. R. E. Powe, C. T. Carley and E. H. Bishop, Free convection flow patterns in cylindrical annuli, *Trans. Am. Soc. Mech. Engrs., Series C, J. Heat Transfer* **91,** 310 (1969).
4. C. Y. Liu, W. K. Mueller and F. Landis, Natural convection heat transfer in long horizontal cylindrical annuli, *International Developments in Heat Transfer*, paper no. 117, part V, pp. 976–984 (1969).
5. E. H. Bishop and C. T. Carley, Photographic studies of natural convection between concentric cylinders, *Proc. of the* 1966 *Heat Transfer and Fluid Mechanics Institute.* Stanford University Press, pp. 63–78 (1966).
6. U. Grigull and W. Hauf, Natural convection in horizontal cylindrical annuli, *Proc. of the Third International Heat Transfer Conference*, paper no. 60, vol. 2, pp. 182–195 (1966).
7. J. Lis, Experimental investigation of natural convection heat transfer in simple and obstructed horizontal annuli, *Proc. of the Third International Heat Transfer Conference*, paper no. 61, vol. 2, pp. 196–204 (1966).
8. T. H. Kuehn and R. J. Goldstein, An experimental and theoretical study of natural convection in the annulus between horizontal concentric cylinders, *J. Fluid Mech.* **74,** 695–719 (1976).
9. T. H. Kuehn and R. J. Goldstein, Numerical solution to the Navier–Stokes equations for laminar natural convection about a horizontal isothermal circular cylinder, *Int. J. Heat Mass Transfer* **23,** 971–979 (1980).
10. S. H. Yin, R. E. Powe, J. A. Scanlan and E. H. Bishop, Natural convection flow patterns in spherical annuli, *Int. J. Heat Mass Transfer* **16,** 1785–1795 (1973).
11. S. N. Singh and J. T. Chen, Numerical solution for natural convection between concentric spheres at moderate Grashof numbers, *Numer. Heat Transfer* **3,** 441–459 (1980).
12. L. R. Mack and H. C. Hardee, Natural convection between concentric spheres at low Rayleigh numbers, *Int. J. Heat Mass Transfer*, **11,** 387–396 (1968).
13. J. H. Lee and T. S. Lee, Natural convection in the annuli between horizontal confocal elliptical cylinders, *Int. J. Heat Mass Transfer* **24,** 1739–1742 (1981).
14. F. N. Lin and B. T. Chao, Laminar free convection over two-dimensional and axisymmetric bodies of arbitrary contour, *Journal Heat Transfer* **96,** 435–442 (1974).
15. A. J. Ede, *Advances in Heat Transfer*, vol. 4, pp. 1–64. Academic Press, New York (1967).

APPENDIX 1

Nusselt number determination on isothermal surfaces described by elliptical coordinates.

An energy balance at a solid surface yields,

$$Nu = -2\nabla \cdot T.$$

In terms of the elliptical coordinate system,

$$\nabla \cdot T = \frac{\left[\left(\cosh(\xi)\sin(\eta)\frac{\partial T}{\partial \xi} + \sinh(\xi)\cos(\eta)\frac{\partial T}{\partial \eta}\right)^2 + \left(\sinh(\xi)\cos(\eta)\frac{\partial T}{\partial \xi}\cosh(\xi)\sin(\eta)\frac{\partial T}{\partial \eta}\right)^2\right]^{1/2}}{\sinh^2(\xi)\cos^2(\eta) + \cosh^2(\xi)\sin^2(\eta)}.$$

For an isothermal surface,

$$\frac{\partial T}{\partial \eta} = 0$$

$$Nu = \frac{-2\dfrac{\partial T}{\partial \xi}}{[\sinh^2(\xi)\cos^2(\eta) + \cosh^2(\xi)\sin^2(\eta)]^{1/2}}.$$

The average Nusselt number is given by:

$$\overline{Nu} = \frac{\oint Nu(\eta)\,ds}{\oint ds}$$

$$= \frac{-2\pi F_o'}{\int_0^{\pi} [\cosh^2(\xi)\sin^2(\eta) + \sinh^2(\xi)\cos^2(\eta)]^{1/2}\,d\eta}.$$

APPENDIX 2: SERIES SOLUTION IN TERMS OF POWERS OF Ra_L

Into the partial differential equations derived in the formulation section are substituted the power series for the two dependent variables:

$$T = T_0 + RaT_1 + Ra^2T_2 + Ra^3T_3 + \cdots$$

$$\psi = Ra\psi_1 + Ra^2\psi_2 + Ra^3\psi_3 + \cdots$$

where

$$\zeta = -\nabla^2\psi.$$

This substitution yields three equations for each power of Ra_L plus the equation for pure conduction. The equation

derived for the first two powers of Ra_L are:

Conduction equation

$$\nabla^2 T_0 = 0$$

Ra^1:

$$\frac{\partial^2 \zeta_1}{\partial \xi^2} + \frac{\partial^2 \zeta_1}{\partial \eta^2} = -\left(\frac{r_i}{L}\right)^3 (\cos(\alpha)\cos(\eta)\sinh(\xi) - \sinh(\alpha)\sin(\eta)\cosh(\xi))\frac{\partial T_0}{\partial \xi}$$

$$\zeta_1 = -\nabla^2 \psi_1$$

$$\frac{\partial^2 T_1}{\partial \xi^2} + \frac{\partial^2 T_1}{\partial \eta^2} = \frac{\partial T_0}{\partial \xi}\frac{\partial \psi_1}{\partial \eta}$$

Ra^2:

$$\frac{\partial^2 \zeta_2}{\partial \xi^2} + \frac{\partial^2 \zeta_2}{\partial \eta^2} = \frac{1}{Pr}\frac{\partial(\psi_1, \nabla^2 \psi_1)}{\partial(\xi, \eta)} - \left(\frac{r_i}{L}\right)^3 \times \left[(\cos(\alpha)\cos(\eta)\sinh(\xi) - \sin(\alpha)\sin(\eta)\cosh(\xi))\frac{\partial T_1}{\partial \xi}\xi - \sin(\alpha)\cos(\eta)\sinh(\xi) + \cos(\alpha)\sin(\eta)\cosh(\xi)\frac{\partial T_1}{\partial \xi}\right]$$

$$\zeta_2 = -\nabla^2 \psi_2$$

$$\frac{\partial^2 T_2}{\partial \xi^2} + \frac{\partial^2 T_2}{\partial \eta^2} = \frac{\partial(T_1, \psi_1)}{\partial(\xi, \eta)} + \frac{\partial(T_0, \psi_2)}{\partial(\xi, \eta)}$$

where

$$\nabla^2 \psi_j = \frac{1}{\sinh^2 \xi \cos^2 \eta + \cosh^2 \xi \sin^2 \eta} \times \left[\frac{\partial^2 \psi_j}{\partial \xi^2} + \frac{\partial^2 \psi_j}{\partial \eta^2}\right].$$

The coefficients of the increasing powers of Ra are determined by solving the equations sequentially. In each instance, this procedure yields three Poisson equations to be solved per each higher power of the Rayleigh number.

While this procedure is not difficult in principle, the expressions for the inhomogenities of each equation become progressively more difficult for each successively higher order of Ra. This successive complexity is particularly great in the problem treated here. The elliptical coordinate system can be viewed as a generalized version of a polar coordinate system. This greater generality in the form of the parameter of an arbitrary eccentricity presents expressions which are intractable from a practical standpoint for all but the first power of Ra.

CONVECTION NATURELLE ENTRE DEUX CYLINDRES ELLIPTIQUES CONFOCAUX ET HORIZONTAUX

Résumé—La convection naturelle stationnaire bidimensionnelle dans un espace annulaire entre deux cylindres elliptiques confocaux, orientés selon un angle α par rapport à la force de pesanteur, est exprimée dans un système de coordonnées elliptiques. La méthode du développement spectral en série est utilisée pour réduire les équations aux dérivées partielles à trois systèmes d'équations différentielles du second ordre. Ces équations sont tronquées puis intégrées numériquement en utilisant un code COLSYS [1] de collocation à éléments finis pour des équations différentielles à valeurs limites. Des conductivités globales équivalentes pour les surfaces internes sont déterminées pour: nombre de Rayleigh basé sur la largeur de l'espacement Ra_L = 100, 1000, 10000; excentricité de l'ellipse interne, e = 0,0, 0,5 et 1,0; nombre de Prandtl, Pr = 0,7; et différents angles d'orientation α de l'anneau elliptique par rapport à la gravité. Le cas spécial e = 1,0 qui correspond à l'écoulement convectif dans l'espace annulaire formé par une ellipse entourant une plaque plane est étudié en détail. Les résultats sont présentés en fonction des configurations de l'écoulement, isothermes, graphes de vorticité et des nombres de Nusselt locaux sur la surface de la plaque pour différentes valeurs de alpha.

NATÜRLICHE KONVEKTION ZWISCHEN WAAGERECHTEN KONFOKAL-ELLIPTISCHEN ZYLINDERN

Zusammenfassung—Das Problem der stationären zweidimensionalen natürlichen Konvektion im Ringraum zwischen zwei konfokal-elliptischen Zylindern, die in einem beliebigen Winkel α bezüglich der Richtung der Schwerkraft angeordnet sind, wird in einem elliptischen Koordinatensystem formuliert. Die Methode der spektralen Reihenentwicklung wird angewandt, um die partiellen Differentialgleichungen in drei Sätze von normalen Gleichungen 2. Ordnung zu überführen. Diese Gleichungen werden abgekürzt und dann mit Hilfe von COLSYS, einem Finite-Elemente-Programm für Randwertprobleme [1], numerisch integriert. Äquivalente Leitfähigkeiten, bezogen auf die innere Oberfläche, werden für folgende Fälle bestimmt: Rayleigh-Zahl, bezogen auf die Spaltweite: Ra_L = 100, 1000, 10000; Exzentrizität der inneren Ellipse: e = 0,0, 0,5, 1,0; Prandtl-Zahl: Pr = 0,7; verschiedene Orientierungswinkel α des elliptischen Ringraums. Der Spezialfall von e = 1,0, der einem Ringraum zwischen einer ebenen Platte (innen) und einem elliptischen Zylinder (außen) entspricht, wird genauer untersucht. Die Ergebnisse werden in Form von Stromlinien, Isothermen, Wirbelbildern und örtlichen Nusselt-Zahlen an der Plattenoberfläche für verschiedene Werte von α dargestellt.

ЕСТЕСТВЕННАЯ КОНВЕКЦИЯ МЕЖДУ КОНФОКАЛЬНЫМИ ГОРИЗОНТАЛЬНЫМИ ЭЛЛИПТИЧЕСКИМИ ЦИЛИНДРАМИ

Аннотация—В эллиптической системе координат сформулирована задача об установившейся двумерной естественной конвекции в кольцевом слое, образованном конфокальными эллиптическими цилиндрами, которые составляют произвольный угол α относительно силы тяжести. Используется метод спектрального разложения в ряды, чтобы свести определяющие связанные дифференциальные уравнения в частных производных к трем системам обыкновенных уравнений второго порядка. Эти уравнения укорочены и затем численно интегрируются с помощью COLSYS [1], которая является конечно-элементным коллокационным кодом для дифференциальных уравнений на границах. Суммарные эквивалентные проводимости для внутренней поверхности определяются для чисел Рэлея, основанных на ширине зазора, $Ra_L = 100$, 1000 и 10000; эксцентриситета внутреннего эллипса, $e = 0{,}0$, 0,5 и 1,0; числа Прандтля, $Pr = 0{,}7$, и различных углах ориентации α эллиптического кольцевого слоя относительно g. Детально исследуется случай $e = 1{,}0$, соответствующий конвекции внутри кольцевого слоя, образованного эллипсом, который окружает плоскую спластину. Результаты содержат структуру течения жидкости, изотермы, распределение завихренности и локальных чисел Нуссельта на поверхности пластины для различных значений α.